

# Stellar populations of LBGs at $z \sim 5$ II : The stellar mass function and the stellar mass density

Kiyoto Yabe<sup>1</sup>, Kouji Ohta<sup>1</sup>, Ikuru Iwata<sup>2</sup>, Marcin Sawicki<sup>3</sup>, Naoyuki Tamura<sup>4</sup>, Masayuki Akiyama<sup>5</sup>, Kentaro Aoki<sup>4</sup>

1. Kyoto Univ.  
2. NAOJ, Okayama  
3. St. Mary's Univ.  
4. NAOJ, Hawaii  
5. Tohoku Univ.

## Abstract

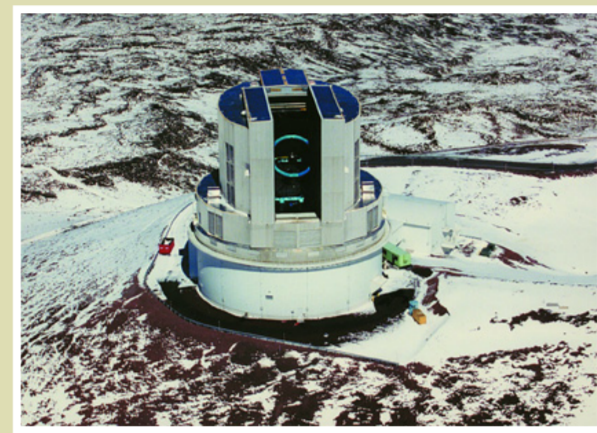
We present the results of SED fitting analysis for Lyman Break Galaxies at  $z \sim 5$  in the GOODS-N and its flanking fields. With the IRAC images in the GOODS-N, which are publicly available, and the IRAC images that we observed in the flanking fields, we constructed the rest-frame UV-optical SEDs for our large sample that is selected robustly. For this sample, we fit the observed SEDs with population synthesis models. By using the large sample of galaxies at  $z \sim 5$ , we derived a stellar mass function by correcting for incompleteness. By integrating down to  $10^8 M_{\text{sun}}$ , the stellar mass density at  $z \sim 5$  is calculated to be  $(0.7-2.4) \times 10^7 M_{\text{sun}} \text{Mpc}^{-3}$ .

## I. Objective

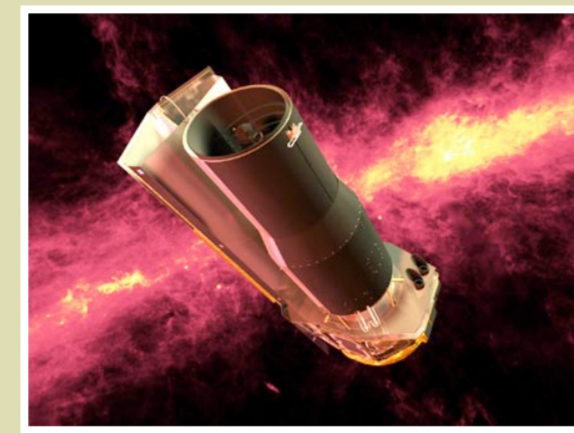
Recent studies show the gradual increase of the stellar mass density with time. However, the studies on the stellar mass of galaxies at  $z > 5$  are restricted because the lack of sufficiently deep mid-IR data. With the advent of Spitzer, we can access the rest-frame optical wavelength, and thus, the stellar mass of galaxies at  $z \sim 5$ . In this presentation, we explore the properties, especially stellar mass, of Lyman Break Galaxies (LBGs) at  $z \sim 5$  using Subaru/S-Cam and Spitzer/IRAC imaging data.

## 2. Sample Selection

We use the LBG sample of Iwata et al. (2007), which consists of  $\sim 600$  objects in/around the GOODS-N. Among them, we select objects which appear to be isolated and not contaminated by neighboring objects in IRAC images. With the public IRAC images in the GOODS-N and the IRAC images we observed in the GOODS-FF, we constructed observed SEDs for the large sample selected robustly, which consists of  $\sim 100$  objects.

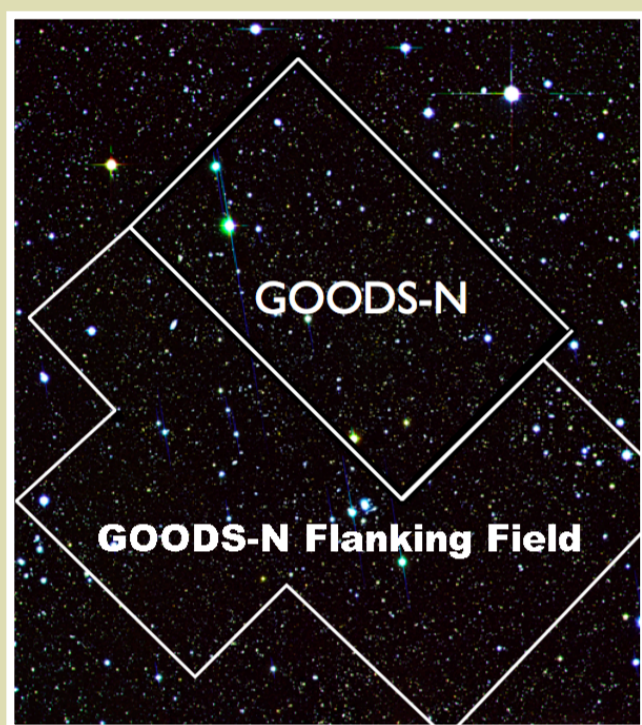


**Subaru/Suprime-Cam**  
Effective area:  $\sim 500 \text{ arcmin}^2$   
Magnitude limit ( $1.2'' \Phi, 5\sigma$ ):  
V:28.2, Ic:26.9, z':26.6

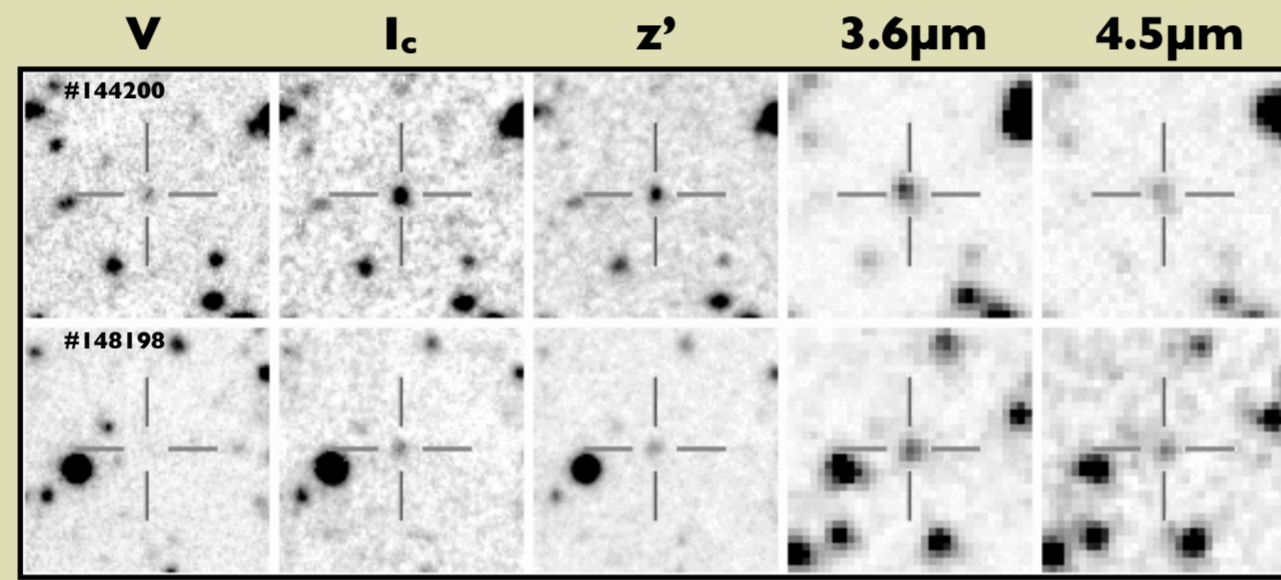


**Spitzer/IRAC**  
Effective area:  $\sim 400 \text{ arcmin}^2$   
Magnitude limit ( $2.4'' \Phi, 3\sigma$ ):  
3.6 $\mu\text{m}$ :25.9, 4.5 $\mu\text{m}$ :25.6 (GOODS-N)  
3.6 $\mu\text{m}$ :24.8, 4.5 $\mu\text{m}$ :24.1 (GOODS-FF)

In the bottom figure, two example images of our sample are shown. These objects are selected robustly to make reliable photometry.



Area covered by IRAC is presented on the Subaru/Suprime-Cam area. Almost 80% of the optical images is covered by the mid-Infrared images.



The postage stamps of objects in 5 passbands. The LBG candidate is indicated by a cross in each panel.

## 3. Population Synthesis Modeling

population synthesis modeling is handled as follows:

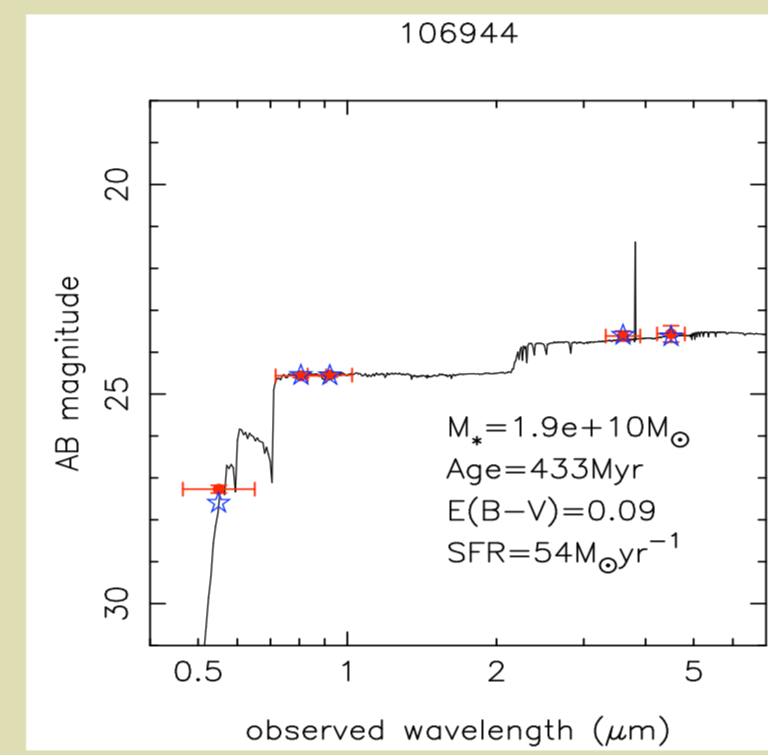
- Bruzual & Charlot 2003
- Salpeter IMF (0.1 -  $100 M_{\text{sun}}$ )
- Constant Star Formation History
- 0.2  $Z_{\text{sun}}$  model
- Calzetti extinction law
- Including H $\alpha$  emission
- Redshift of all objects is fixed to be  $z=4.8$

Note:

- H $\alpha$  emission line is included in the model spectrum with Kennicutt law.
- We examine the effects of these model assumptions (choice of star formation history, metallicity, extinction law) on the stellar mass and found the effects is  $\sim 0.3 \text{ dex}$  at most.

## 4. Results

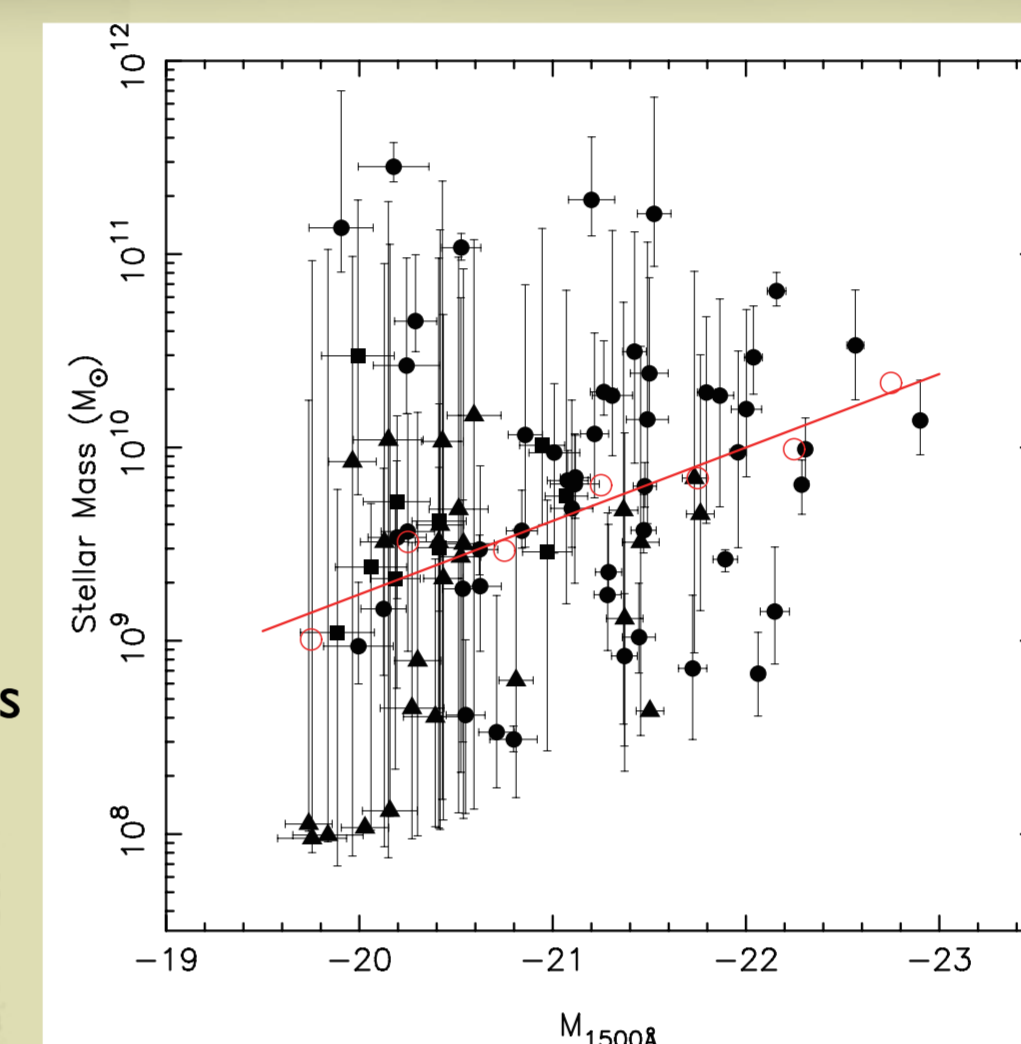
Comparing the observed SEDs with model SEDs, we infer the stellar properties of galaxies at  $z \sim 5$ . In the bottom-left figure, an example of our fitting result is presented with the output parameters.



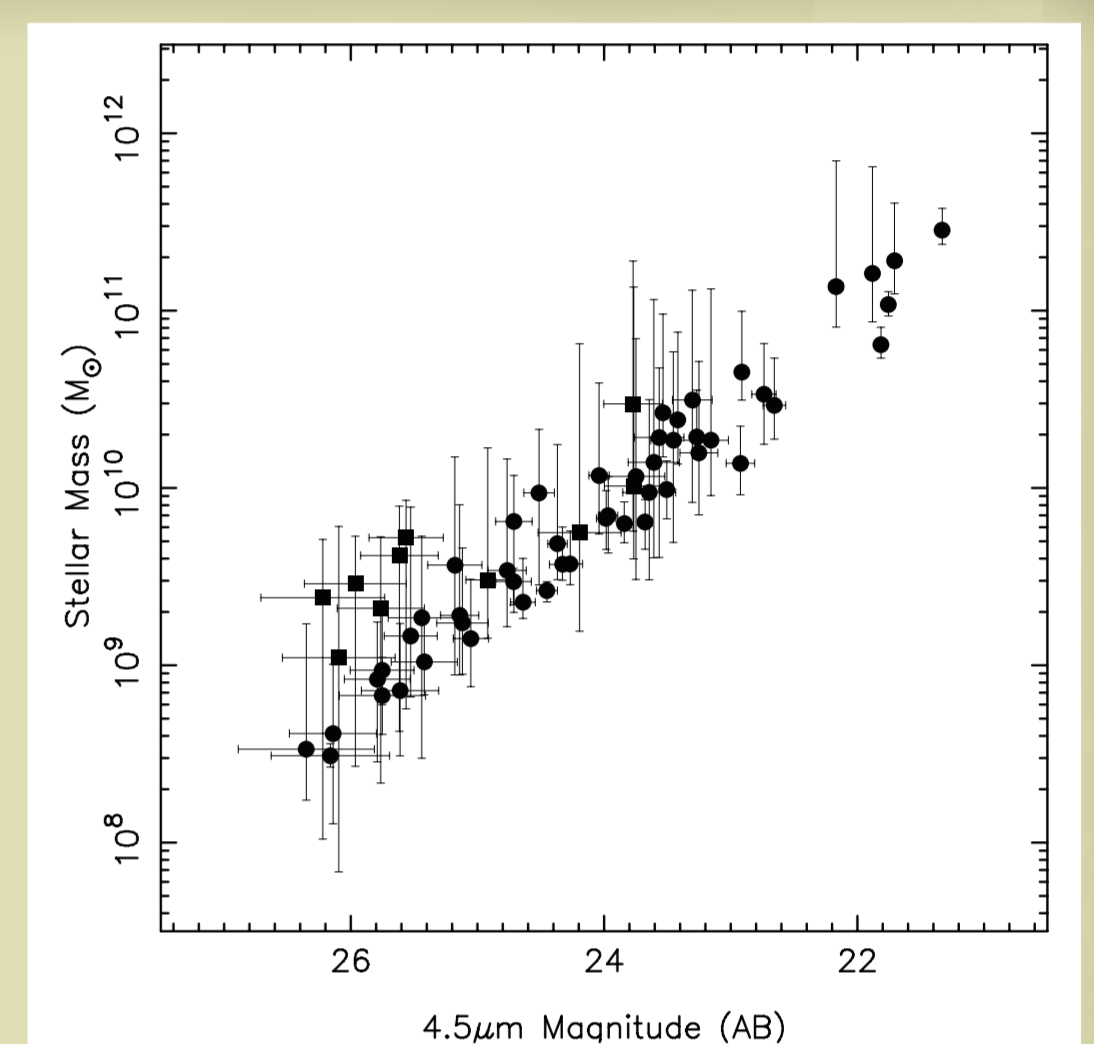
A best-fitted 0.2 $Z_{\text{sun}}$ , CSF model. The observed SED and the model SED are indicated by red points and blue points, respectively. The best-fitted parameters are also shown.

Sample best-fitted parameters

$$\begin{aligned} M_{* \text{ median}} &= 4.1 \times 10^9 M_{\text{sun}} \\ \text{Age}_{\text{ median}} &= 25 \text{ Myr} \\ E(B-V)_{\text{ median}} &= 0.22 \text{ mag} \\ \text{SFR}_{\text{ median}} &= 141 M_{\text{sun}} \text{ yr}^{-1} \end{aligned}$$



$M_{1500\text{Å}}$  vs. stellar mass. Objects detected both in 3.6 $\mu\text{m}$  and 4.5 $\mu\text{m}$  are indicated by circles. Objects detected only in 3.6 $\mu\text{m}$  (4.5 $\mu\text{m}$ ) are indicated by triangles (squares). Open circles show median stellar mass in 0.5 mag bin.



4.5 $\mu\text{m}$  magnitude vs. stellar mass. Objects detected both in 3.6 $\mu\text{m}$  and 4.5 $\mu\text{m}$  are indicated by circles. Objects detected only in 4.5 $\mu\text{m}$  are indicated by squares.

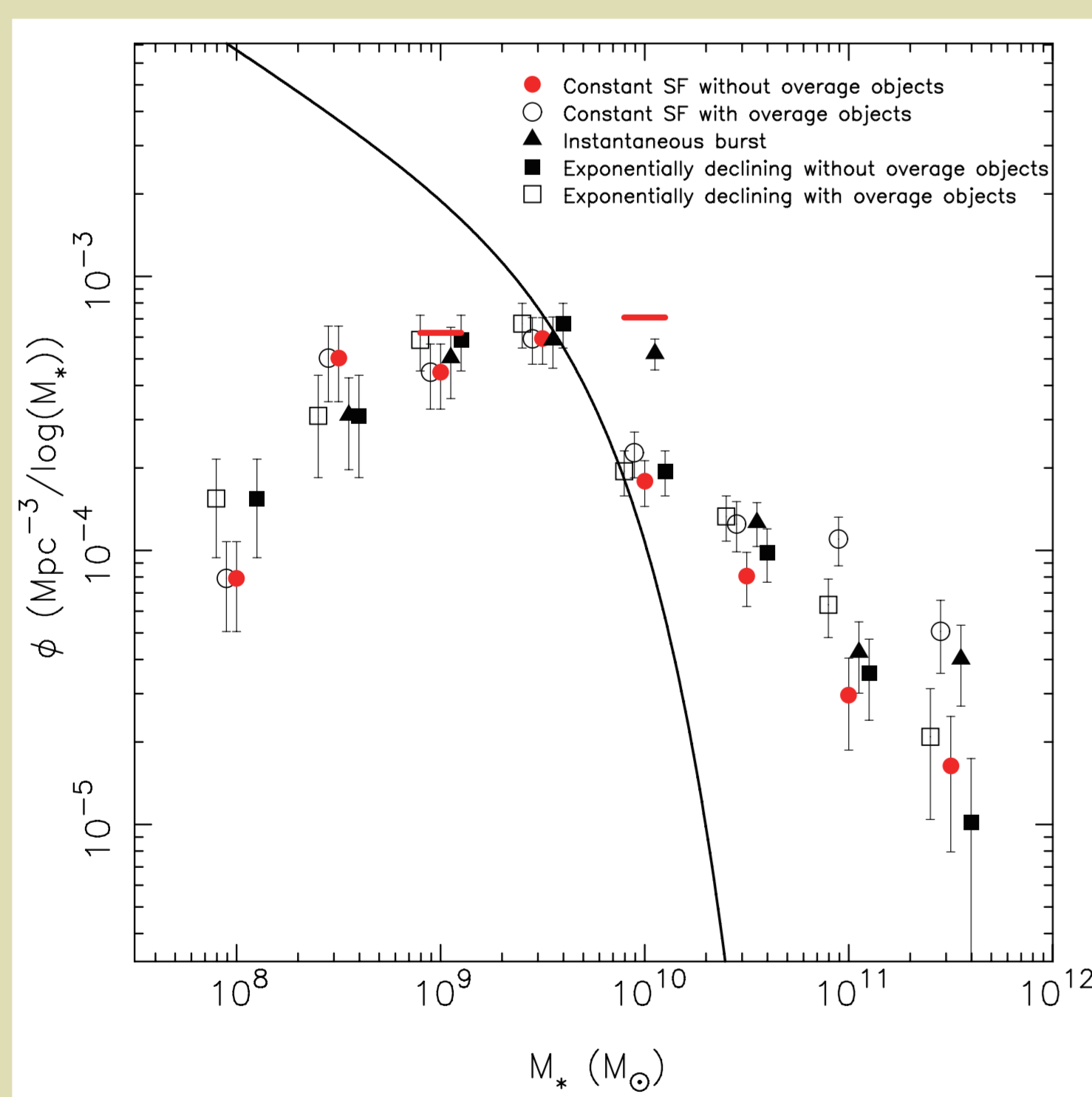
In upper-left figure,  $M_{1500\text{Å}}$  vs. stellar mass plot is presented. The  $M_{1500\text{Å}}$  vs.  $M_{* \text{ median}}$  shows a loose correlation between the rest-frame UV luminosity and stellar mass. In upper-right figure, a tight correlation between the rest-frame optical luminosity and stellar mass is shown.

## 5. The Stellar Mass Function

The large sample of LBGs whose stellar mass is estimated robustly allows us to derive the stellar mass function of LBGs at  $z \sim 5$ . The stellar mass function is calculated by following equation:

$$\phi(\log(M_{*}/M_{\odot})) = \sum_{i,j} \frac{N_{i,j}(1 - f_i^{\text{int}})}{f_{\text{sel}}^{\text{det}} V_i^{\text{eff}} \Delta \log(M_{*}/M_{\odot})}$$

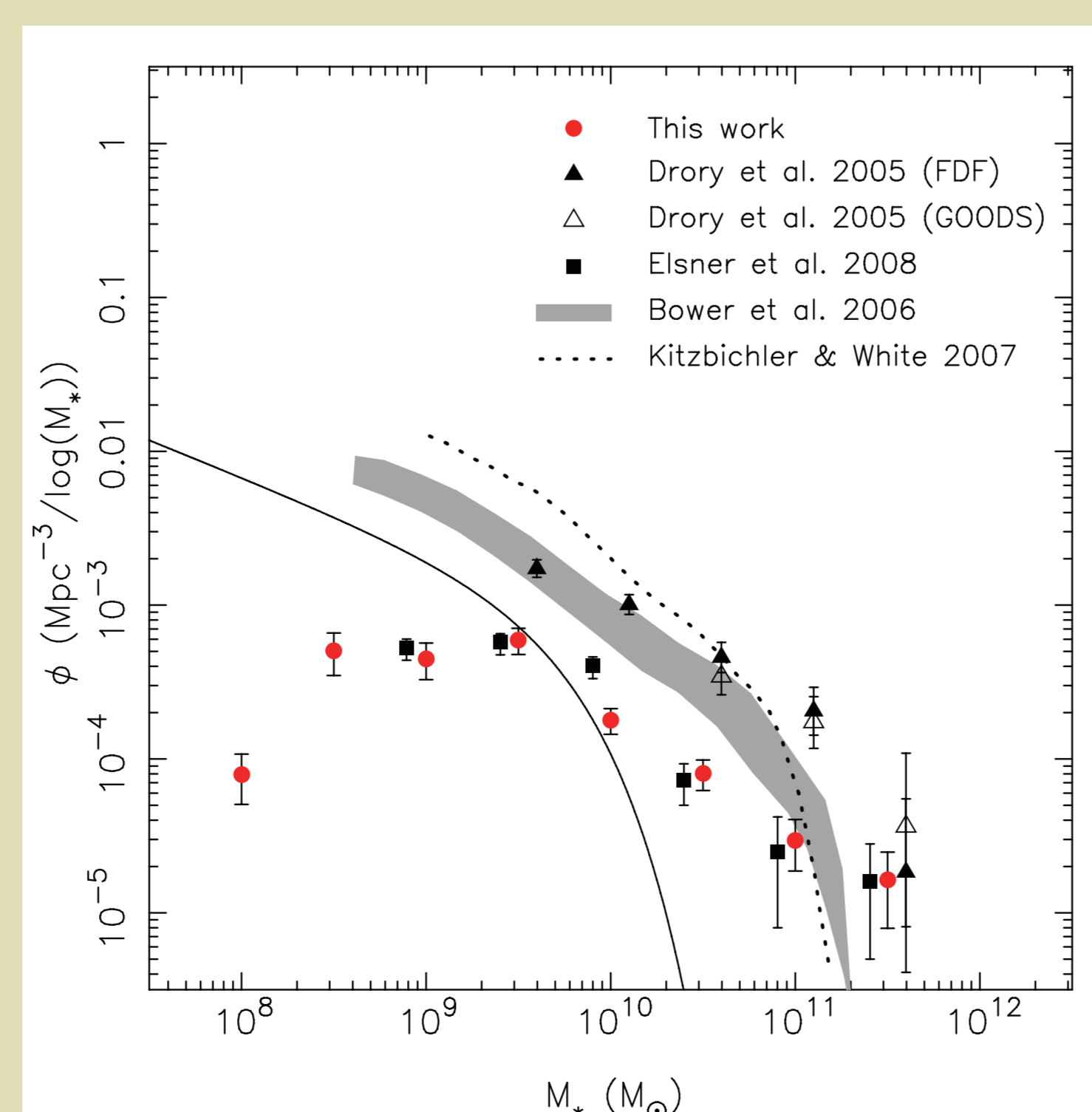
, where  $N_{i,j}$  is the number of objects entering each  $z'$  and 4.5 $\mu\text{m}$ -band bin.  $f_i^{\text{int}}$  refers to a fraction of interlopers estimated  $i$ -th  $z'$ -band bin by Iwata et al. (2007) and  $f_{\text{sel}}^{\text{det}}$  is a fraction of uncontaminated objects in IRAC images.  $f_i^{\text{det}}$  is a detection rate in the IRAC 4.5 $\mu\text{m}$ -band and  $V_i^{\text{eff}}$  is an effective volume as a function of  $z'$ -band magnitude taken from Iwata et al. (2007).



The stellar mass functions of LBGs at  $z \sim 5$  assuming various star formation histories (constant star formation: circle, instantaneous burst: triangle,  $\tau$ -model: square). The mass function excluding objects whose fitted age is larger than the cosmic age at  $z=4.8$  is indicated by filled symbols. The horizontal bars indicate the plausible number densities including objects detected neither in 3.6 $\mu\text{m}$  nor 4.5 $\mu\text{m}$ . Also the expected stellar mass function from the UVLF is indicated by a solid line.

The derived stellar mass functions assuming various star formation histories are plotted in the left figure. Although uncertainties remain, the stellar mass function we present in this work is that derived with constant star formation history and excluding objects whose fitted ages exceed the cosmic age at  $z \sim 5$ .

The stellar mass function estimated from the rest-frame UVLF by Iwata et al. (2007) and the rough correlation between the rest-frame UV magnitude and the stellar mass is plotted as a solid curve in the left figure. Also the expected number densities for objects undetected in 3.6 $\mu\text{m}$  and 4.5 $\mu\text{m}$ -band are indicated red horizontal bars.

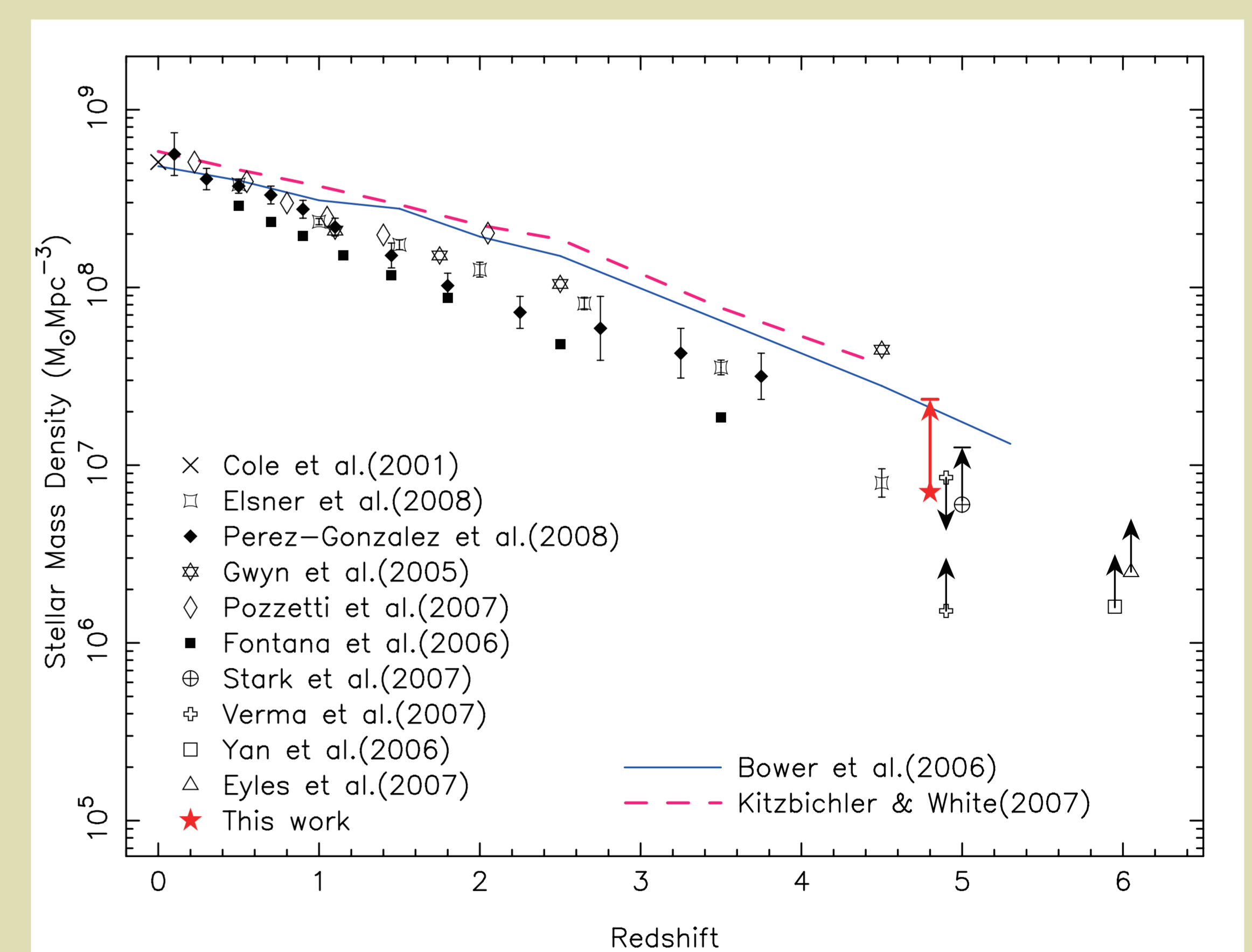


Comparison of the stellar mass function of our sample with other observations and theoretical models. The expected stellar mass function from the UVLF is indicated by a solid line.

As illustrated in the right figure, the stellar mass function for our sample is consistent with that for the sample by Elsner et al. (2007). The stellar mass function disagrees with the results by Drory et al. (2005) except in the most massive part. Our results and theoretical models agree at the massive end but disagree in other mass bins.

## 6. The Stellar Mass Density

By integrating the stellar mass function down to  $M_{*} = 10^8 M_{\text{sun}}$ , the cosmic stellar mass density at  $z \sim 5$  is calculated to be  $(0.7-2.4) \times 10^7 M_{\text{sun}} \text{Mpc}^{-3}$ , which is about 1.4% of the local stellar mass density of Cole et al. (2001).



The cosmic stellar mass density as a function of redshift. The data point for our  $z \sim 5$  sample is plotted with other observations at various redshifts. Our result is indicated by a red star and the plausible upper limit is shown with a horizontal bar. Also, theoretical predictions from semi-analytical models and hydrodynamics simulations are plotted with observed data. All observed values and models of Bower et al. (2006) and Kitzbichler & White (2007) are integrated down to  $10^8 M_{\text{sun}}$ .

In the above figure, comparison with other observational works and theoretical predictions of semi-analytic models is shown. All data points are values integrated down to  $10^8 M_{\text{sun}}$  and calculated by using the same Salpeter IMF and cosmological parameters.

Our data point is consistent with the general trend of the increase of stellar mass density with time. Also our stellar mass density is almost comparable to the models if we take into account the plausible upper limit.